Synthesis and characterization of Fe/Co/Ni alloys–MgO nanocomposite powders

Valérie Carles, Christophe Laurent,* Marc Brieu and Abel Rousset

Laboratoire de Chimie des Matériaux Inorganiques, ESA CNRS 5070, Université Paul-Sabatier, 31062 Toulouse cedex 4, France. E-mail: laurent@iris.ups-tlse.fr

A mixed oxalate β-$Mg_{0.896}Fe_{0.047}Co_{0.034}Ni_{0.023}C_2O_4 \cdot 2H_2O$ of well controlled size and morphology was prepared by coprecipitation. The corresponding quaternary solid solution between MgO, FeO, CoO and NiO was prepared by thermal decomposition and calcination in a $H_2/H_2O/N_2$ atmosphere. The selective reduction of the solid solution in an H_2 atmosphere was studied by a combination of X-ray diffraction, Mössbauer spectroscopy, transmission electron microscopy and associated analysis. This work has brought to light the very high stability of Fe^{2+}, Co^{2+} and notably Ni^{2+} when substituted for Mg^{2+} in the MgO rocksalt lattice. It is necessary to perform the reduction at 1300 °C fully to reduce the transition metal ions. The alloy particles are either distributed as relatively large particles (tens to hundreds of nanometers) at the surface of the MgO grains or as much smaller particles ($\leqslant 20$ nm) probably located inside the matrix grains and epitaxial with it. The composition distribution of the large surface particles is fairly broad when the reduction was performed at 1100 and 1300 °C. In contrast, it is much narrower in the powder prepared by reduction at 1200 °C, although the particles are still low in Ni compared to the target composition.

Introduction

Nanocomposite materials have been widely studied in recent years owing to their potentially interesting properties.[1–4] In particular, the dispersion of metal nanoparticles in an inorganic matrix has aroused great interest. Metal–oxide nanocomposite powders have been prepared by direct reactions between the appropriate reagents by several routes such as the sol–gel method,[5] mechanical alloying[6] and combustion synthesis.[7] These methods generally do not allow a precise control of the microstructure of the composite powders, notably with respect to the size and composition of the metal particles. In contrast, the present laboratory has proposed an original method[8] based on the selective reduction in H_2 of homogeneous oxide solid solutions in order to prepare metal–oxide nanocomposite powders. Different composite systems have been investigated: (Fe, Cr, Ru)–Al_2O_3,[8–11] (Fe, Cr)–Cr_2O_3,[12] (Fe, Ni)–MgO[13,14] and (Fe, Co, Ni)–$MgAl_2O_4$.[15,16] In these powders, most of the metallic phase is found in the form of nanometric particles dispersed within the oxide grains or at their surface. It has been shown that several factors such as the transition metal content, the mutual solubility of the parent oxides, the specific surface area and the crystalline state of the starting oxide solid solution can modify the size, the size distribution and the location (inside or at the surface of the oxide grains) of the metal particles. In addition, it is possible to control, to a certain extent, the composition of the nanoparticles in the case of binary alloys (Fe/Cr, Fe/Ru, Fe/Co and Fe/Ni).[10–12,14,16] These studies have notably thrown light on the high stability upon reduction of the iron ions substituting in the lattices of Al_2O_3, Cr_2O_3, MgO and $MgAl_2O_4$. However, the presence of other transition metal ions that are more easily reduced to the metallic state has been found to enhance the reducibility of the iron ions. Both ruthenium and nickel favour the reducibility of Fe(III) substituting for Al(III) ions in Al_2O_3.[11] Cobalt enhances the reducibility of Fe(II) substituting for Mg(II) ions in $MgAl_2O_4$.[16] Similarly, the presence of iron favours the reduction of Cr(III) ions substituting for Al(III) ions in Al_2O_3.[10] The reduction temperature is the main parameter that controls the composition of the alloy particles for a given composition of the starting oxide. The nanoparticles are progressively enriched in the less reducible metal as the selective reduction of the oxide solid solution progresses upon the increase in reduction temperature. This temperature is relatively high, in the 800–1300 °C range, in order to reduce oxide solid solutions having a low specific surface area (typically 5–20 $m^2\,g^{-1}$) as required for the dispersion of metal nanoparticles with a small average size and a narrow size distribution. Chatterjee *et al.*[17] have claimed that the H_2 reduction of gel pieces at moderate temperatures could produce Fe/Cr alloy nanoparticles dispersed in silica, but they do not give the composition of their particles.

The present work aims at extending this chemical process to the dispersion of ternary alloy nanoparticles in an oxide matrix. It follows previous works on Fe–MgO[13] and $Fe_{0.65}Ni_{0.35}$–MgO[14] and it will focus on the $Fe_{0.47}Co_{0.31}Ni_{0.22}$–MgO composite powder. This particular composition of the metallic phase was chosen because unsupported $Fe_{0.47}Co_{0.31}Ni_{0.22}$ nanoparticles are known to present a particularly high value of the saturation magnetization and a low value of the coercive force.[18] The first part of the present paper is devoted to the synthesis of the appropriate quaternary solid solution between MgO, FeO, CoO and NiO by the oxalate precursor route that was used for the preparation of binary and ternary solid solutions.[13,14,19] The second part deals with the reduction behaviour of the oxide solid solution and the formation of the composite powder, notably with respect to the composition of the metallic phase.

Experimental

The appropriate amounts of $Mg(NO_3)_2 \cdot 6H_2O$ (5.00 mol l^{-1}), $FeCl_2 \cdot 4H_2O$ (0.26 mol l^{-1}), $NiCl_2 \cdot 6H_2O$ (0.12 mol. l^{-1}) and $CoCl_2 \cdot 6H_2O$ (0.17 mol l^{-1}) were dissolved in deionized water. Hydrochloric acid (35 vol.%) was added to prevent oxidation of the divalent iron ions and hydroxide precipitation. The mixture, heated at 50 °C, was added while stirring to an aqueous solution of $(NH_4)_2C_2O_4 \cdot H_2O$ also maintained at 50 °C (2.38 mol l^{-1}; in stoichiometric quantity with the metal salts). The oxalate so obtained was quickly cooled to ambient temperature and stirred for 1 h at 20 °C. After filtering, alcohol washing and drying overnight at 50 °C, the oxalate was manually ground and passed through a 250 μm sieve. For the sake of comparison, $MgC_2O_4 \cdot 2H_2O$ was prepared using the same conditions [$Mg(NO_3)_2 \cdot 6H_2O$ 5.00 mol l^{-1} and $(NH_4)_2C_2O_4 \cdot$

H_2O 2.14 mol l^{-1}]. The other $MC_2O_4 \cdot 2H_2O$ (M = Fe, Co or Ni) compounds were also prepared and a mechanical mixture of all four simple oxalates in the same proportion of the desired mixed oxalate was made for the sake of comparing the thermal decomposition behaviours. The thermal decomposition of the oxalates was followed in Ar by thermogravimetric (TGA) and differential thermal (DTA) analysis because the apparatus available in the laboratory does not allow one to work in a $H_2/H_2O/N_2$ atmosphere.

The oxide powders were prepared by thermal decomposition at the appropriate temperature (500 °C), as determined by thermogravimetric analyses. The magnesium oxalate was decomposed in flowing N_2 whereas the specimen containing the transition metal cations was decomposed in a flowing controlled $H_2/H_2O/N_2$ atmosphere ($H_2 = 4.6$ mol.%, $H_2O = 2.0$ mol.%, $N_2 = 93.4$ mol.%) to avoid phase partitioning from the MgO-based (rocksalt) structure.[20] This latter specimen will be hereafter denoted by OX500. It was further calcined at 800 °C for 1 h in a controlled H_2O/N_2 atmosphere ($H_2O = 1.5$, $N_2 = 98.5$ mol.%) in order to improve the crystallization state and lower the specific surface area (specimen denoted by OX800 hereafter). Finally, OX800 was reduced in a pure, dry H_2 flow at either 1100, 1200, or 1300 °C for 1 h, giving rise to the metal–oxide nanocomposite powder. These powders will be hereafter designated R1100, R1200 and R1300, respectively. A total reduction of the transition metal ions should yield a 10 wt.% $Fe_{0.47}Co_{0.31}Ni_{0.22}$–MgO composite. This particular metal content was chosen because it is an acceptable compromise between lower amounts, which generally give rise to smaller particles but increase the characterization difficulties, and higher amounts which result in much larger metal particles.

Phase detection and identification was carried out by X-ray diffraction (XRD) pattern analysis ($\lambda_{CoK\alpha} = 0.17902$ nm). Some patterns (not shown) have been recorded using NaCl as an internal standard. The total metal contents in the OX800 oxide were determined by plasma emission spectroscopy with a relative error of about 1 wt.%. The oxalate and oxide powders were observed by scanning electron microscopy (SEM). The specific surface areas of the oxide powders were measured by the Brunauer–Emmett–Teller (BET) method using N_2 adsorption at liquid N_2 temperature. The nanocomposite powders were observed by transmission electron microscopy (TEM). The local metal contents in OX800 and the composition of the alloy particles in the nanocomposite powders were investigated by TEM energy dispersive X-ray (EDX) microanalysis. About twenty spot analyses were performed for a given powder using a 4, 7 or 15 nm diameter probe depending on the size of the metal particles under examination. TEM EDX microanalyses have been performed on metal particles larger than 20 nm in size and located on the edges of the MgO grains. The nature of the iron species present in the oxide solid solutions and in the nanocomposite powders was determined by ^{57}Fe Mössbauer spectroscopy. Spectra were recorded at room temperature (RT) with a constant acceleration spectrometer using a 50 mCi ^{57}Co source in a rhodium matrix. Absolute velocity calibration was carried out with an iron foil with respect to which center shifts (CS) are reported in the text. On the contrary, the Mössbauer spectra are not converted with respect to natural Fe, the CS value of which is given in the corresponding figure caption.

Results and discussion

Oxalate and oxide powders

Analysis of the XRD pattern of the pure magnesium oxalate [Fig. 1(a)] reveals that the precipitation product is the metastable β-$MgC_2O_4 \cdot 2H_2O$ form, in agreement with previous work.[19] Several authors[21,22] have indeed shown that the crystallization can occur in the stable α form or in the metastable
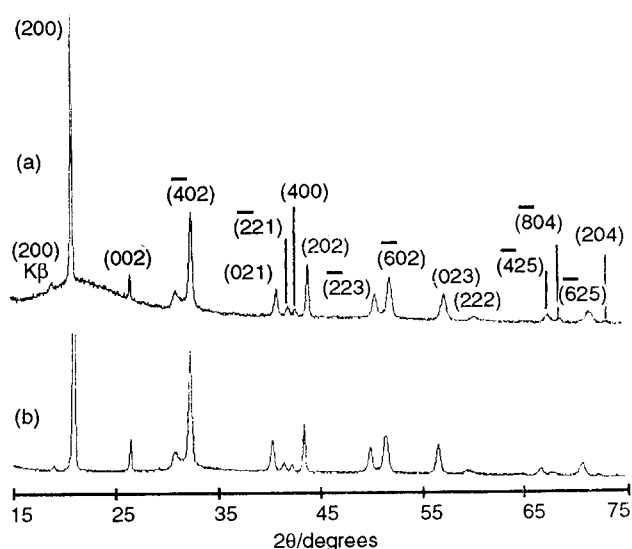

Fig. 1 XRD patterns of β-$MgC_2O_4 \cdot 2H_2O$ (a) and of the mixed oxalate (b).

β form depending on the precipitation conditions. Pezerat et al.[21] claimed that both forms are monoclinic, differing from each other by the presence of stacking faults in the β form. In contrast, Deyrieux and Peneloux[22] claimed that the α and β forms are distinct crystallographic structures differing from each other by the relative positions of the metal–oxalate chains. The pattern of the (Mg, Fe, Co, Ni)–oxalate [Fig. 1(b)] is similar to the former one, no other crystallized phase being detected. This could indicate that the precipitation product indeed is a mixed oxalate rather than a mixture between the simple $MC_2O_4 \cdot 2H_2O$ (M = Mg, Fe, Co or Ni) oxalates, which are known to be isomorphous and crystallize in the monoclinic system.

The DTA and TGA curves relative to the thermal decomposition of both oxalates are shown in Fig. 2(a) and (b). The DTA curves are similar to each other and present two endothermic peaks, the first one of which (ca. 200 °C) could be related to the loss of the 2 constitutional H_2O molecules. The second peak (ca. 465 °C) could correspond to the decomposition of the oxalate group. The TGA curves also reveal that the decomposition takes place in two steps and confirm the above hypothesis. Indeed, the weight losses for the mixed oxalate are equal to the theoretical ones (23.7 and 47.5%) calculated using the experimental contents found for the metallic ions (Mg = 89.6, Fe = 4.7, Co = 3.4, Ni = 2.3 cat.% [where cat. means cationic]). The difference between the latter values and the theoretical ones (Mg = 90.0, Fe = 4.7, Co = 3.1, Ni = 2.2 cat.%) are within the limits of the analysis method. In contrast, the decomposition of the mixture of oxalates [Fig. 2(c)] gives rise to a more complex pattern, involving more than two steps. Thus, it can be concluded from the above results that the present precipitation process has allowed us to prepare a mixed oxalate, the chemical formula of which could be β-$Mg_{0.896}Fe_{0.047}Co_{0.034}Ni_{0.023}C_2O_4 \cdot 2H_2O$.

Analysis of the XRD patterns of MgO [Fig. 3(a)] and of the decomposition product OX500 [Fig. 3(b)] reveals the presence of the same system of peaks, corresponding to the rocksalt lattice. This indicates that OX500 is a monophasic solid solution, the chemical formula of which could be $Mg_{0.896}Fe_{0.047}Co_{0.034}Ni_{0.023}O$. A crystallite size equal to 10 nm was calculated from the XRD pattern using Scherrer's formula. Further calcination at 800 °C only results in a major increase in crystallite size from 10 to a few hundreds of nanometers, as shown by the much narrower peaks on the XRD pattern of OX800 [Fig. 3(c)]. It is noteworthy that the present experimental conditions allow one to avoid any phase partitioning
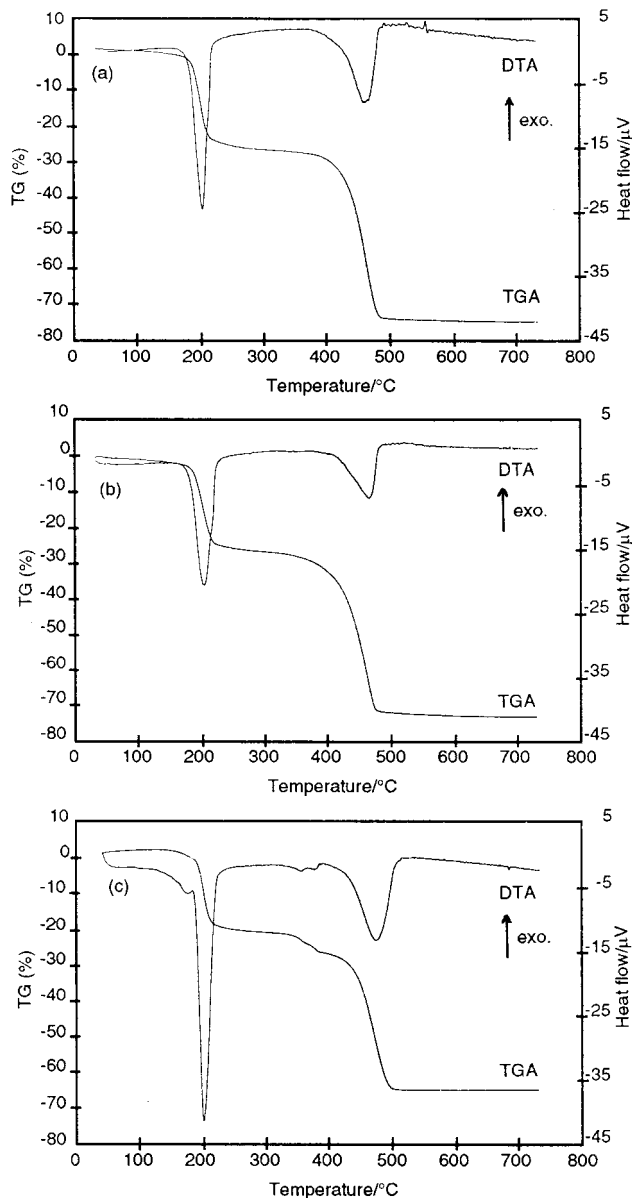
Fig. 2 TGA and DTA curves showing the thermal decomposition of $MgC_2O_4 \cdot 2H_2O$ (a), of the mixed oxalate (b) and of the mixture of oxalates (c).
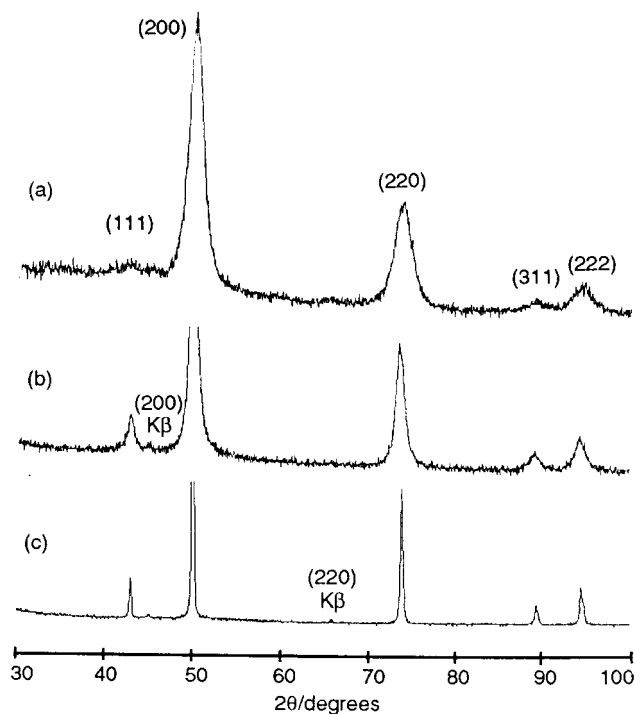

Fig. 3 XRD patterns of pure MgO (a), of the oxide prepared by thermal decomposition at 500 °C (b), and of the oxide calcined at 800 °C (c).
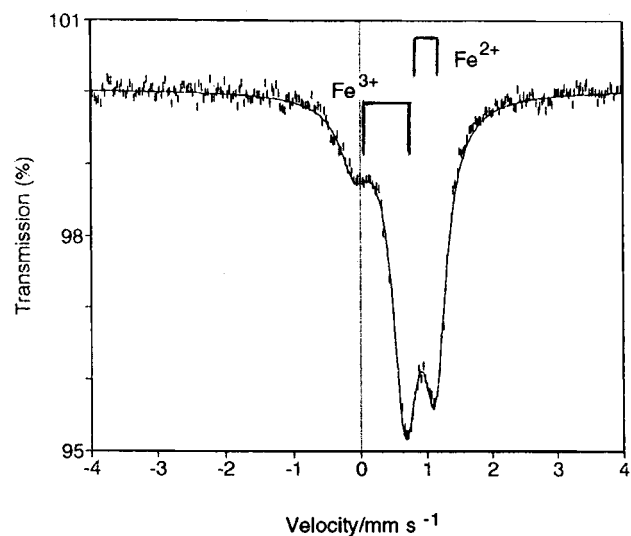

Fig. 4 RT ^{57}Fe Mössbauer spectrum of the oxide calcined at 800 °C; the CS value of natural Fe is equal to -0.15 mm s^{-1}.

and therefore the formation of large overconcentration zones in transition metal within the oxide powders.

The OX800 powder was also studied by RT ^{57}Fe Mössbauer spectroscopy (Fig. 4). The spectrum was fitted assuming it is the sum of a doublet accounting for Fe^{2+} ions (centre shift $CS = 1.08$ mm s^{-1}, half width at half height $\varGamma = 0.22$ mm s^{-1}, quadrupole splitting $\varDelta_{EQ} = 0.48$ mm s^{-1}, proportion $P = 76\%$) and a doublet characteristic of Fe^{3+} ions in the octahedral sites of the rocksalt lattice ($CS = 0.47$ mm s^{-1}, $\varGamma = 0.28$ mm s^{-1}, $\varDelta_{EQ} = 0.90$ mm s^{-1}, $P = 24\%$). Indeed, it is well known that the non-stoichiometric nature of $Fe_{1-\delta}O$ (iron deficiency) provokes the appearing of clusters of cation vacancies V_c'' and Fe^{3+} ions. Waychunas[23] has reported on such clusters in MgO–FeO compounds and noted that observing a quadrupole doublet for the Fe^{2+} ions, as opposed to a singlet, indicates a significant Fe^{2+}–Fe^{3+} pairing. In the present case, Fe^{3+} ions could form by partial oxidation of the Fe^{2+} ions during the thermal treatments in the $N_2/H_2/H_2O$ or H_2O/N_2 atmosphere. In contrast to the results of Waychunas[23] but in agreement with what has been observed for a similar $Mg_{0.9}Fe_{0.1}O$ powder,[19] Fe^{3+} ions located in the tetrahedral sites of the rocksalt lattice have not been detected.

SEM observations [Fig. 5(a)] show that the mixed oxalate powder is made up of agglomerated grains, approximately cubic in shape and about 1 μm in size. As proposed by Tailhades[24] in the case of $FeC_2O_4 \cdot 2H_2O$, the small size of the grains could account for the formation of the metastable β form rather than the stable α form. SEM observation of the OX500 powder reveals the typical pseudomorphism of the thermal decomposition: indeed, the oxide grains are approximately cubic in shape and the average size is close to 0.8 μm [Fig. 5(b)]. Further calcination at 800 °C provokes an important increase in crystallite size, in agreement with the XRD results, and a sintering between the oxide grains [Fig. 5(c)]. Consequently, a major decrease in specific surface area, from 120 to 5 m^2 g^{-1}, is observed as the temperature of calcination of the oxide solid solution is increased from 500 to 800 °C. TEM EDX microanalyses performed on the OX800 powder
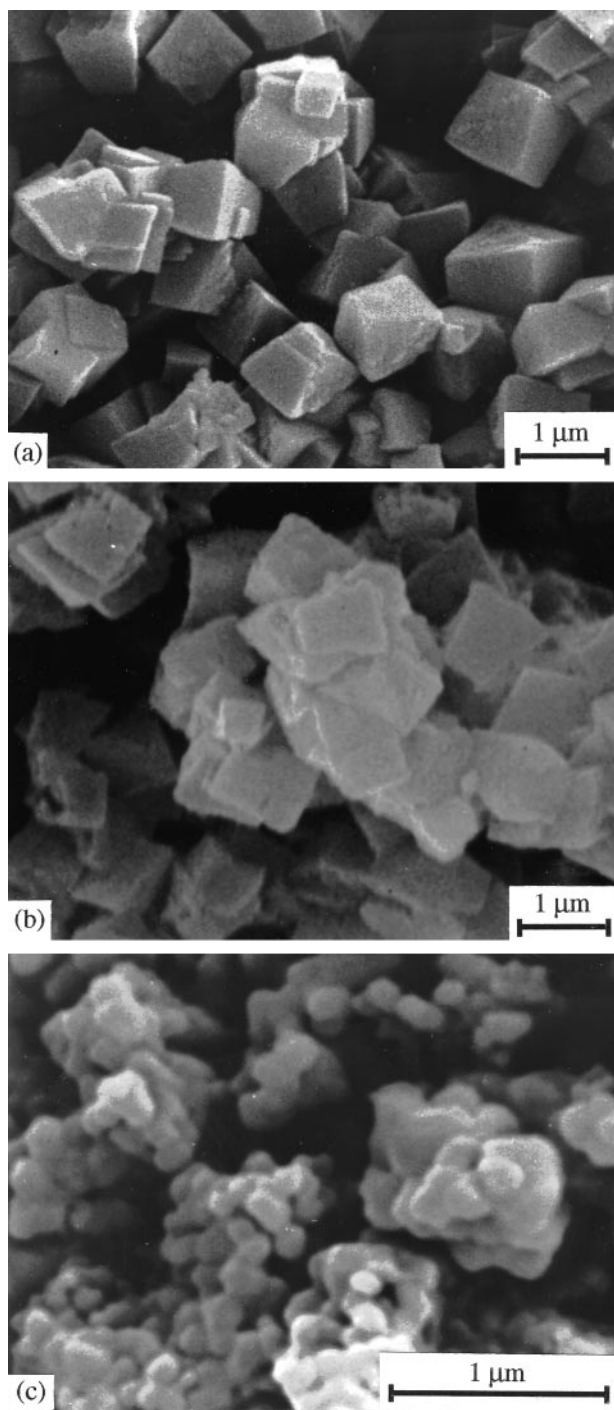
Fig. 5 SEM images of the the mixed oxalate (a), of the oxide prepared by thermal decomposition at 500 °C (b) and of the oxide calcined at 800 °C (c).

confirm the homogeneity of the oxide solid solution, the local contents of Fe, Co and Ni (4.9, 3.5 and 2.3 cat.%, respectively) being close to their respective global contents.

Nanocomposite powders

XRD pattern analysis. XRD pattern analysis of the nanocomposite powders reveals the diffraction peaks of the MgO matrix and the peaks corresponding to one or several metallic phases, depending on the reduction temperature (Fig. 6). The interplanar distance measured for the R1100 powder (0.2025 nm) is close to that of the (110) planes of the body centred cubic (bcc) α-Fe lattice ($d_{110} = 0.2027$ nm). A similar distance is also measured for the R1200 powder (0.2022 nm). Both these peaks could also account for a Fe-
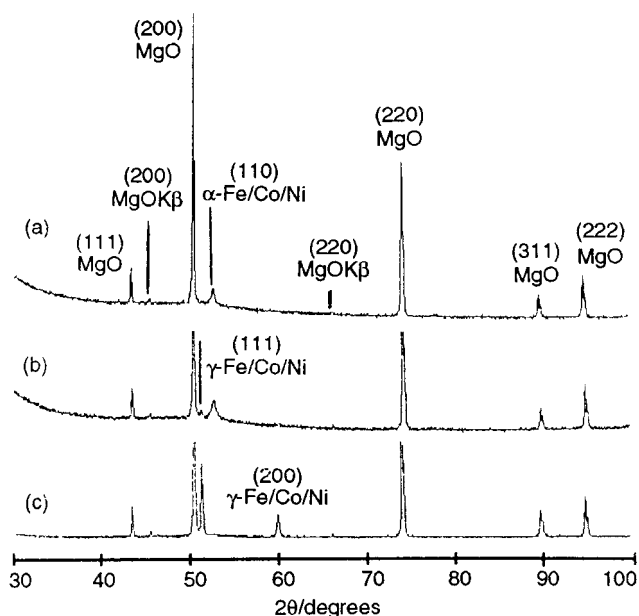

Fig. 6 XRD patterns of the Fe/Co/Ni–MgO nanocomposite powders prepared by reduction at 1100 (a), 1200 (b) or 1300 °C (c).

rich α-Fe/Co/Ni alloy. In addition, a peak (0.2074 nm) that could correspond to the (111) planes of face centred cubic (fcc) γ-Fe/Ni alloys ($d_{111} = 0.208$ nm) is detected for R1200. The interplanar distances measured for the R1300 specimen (0.2071 and 0.1792 nm) could correspond to the (111) and (200) planes of fcc γ-Fe/Ni alloys ($d_{111} = 0.208$, $d_{200} = 0.180$ nm), respectively. Since the presence of a Co-based phase has not been detected in these XRD patterns, it is probable that these alloys also contain Co. The metallic phases obtained by reduction at 1100, 1200 and 1300 °C are in the α, ($\alpha + \gamma$) and γ forms, respectively, which could indicate that the metallic particles get enriched in fcc metals (Ni and/or γ-Co) as the reduction temperature is increased.

[57]Fe Mössbauer spectroscopy. The RT [57]Fe Mössbauer spectra of the R1100, R1200 and R1300 composites and the corresponding Mössbauer parameters are reported in Fig. 7 and Table 1, respectively. The spectra have been fitted with a doublet representing the Fe^{2+} ions in substitution of Mg^{2+} in the MgO lattice and one or more sextets accounting for the ferromagnetic Fe/Co/Ni alloy(s). It should be noted that in the case of R1300 the fit gives a fairly poor description of the spectrum. It was not attempted to improve the fits, notably by using hyperfine-field distributions, because there are several populations for the composition of the Fe/Co/Ni particles as discussed later. In line with earlier results on Fe–MgO,[13] Fe^{3+} ions have not been detected showing that they have been totally reduced to the divalent or metallic state at a temperature lower than or equal to 1100 °C. In contrast, Fe^{3+} ions were still detected in a $Fe_{0.65}Ni_{0.35}$–MgO powder reduced at 1100 °C,[14] which indicated that the presence of nickel was detrimental to the reduction of iron. Thus, the present results may indicate that cobalt favours the reduction of iron and that its effect is strong enough to offset that of Ni. The proportion of Fe^{2+} ions sharply decreases from 44 to 18% upon increasing the reduction temperature from 1100 to 1200 °C. For the R1300 specimen, lines 3 and 4 of the sextet have a very similar intensity, showing that the proportion of Fe^{2+} ions is very small. Despite the fact that the spectrum of the latter specimen, and therefore the corresponding fit, is fairly poor and should be considered with utmost caution, this result is in acceptable agreement with the TEM EDX microanalyses present in a following section showing that the proportion of residual iron ions in the matrix is very low (*ca.*
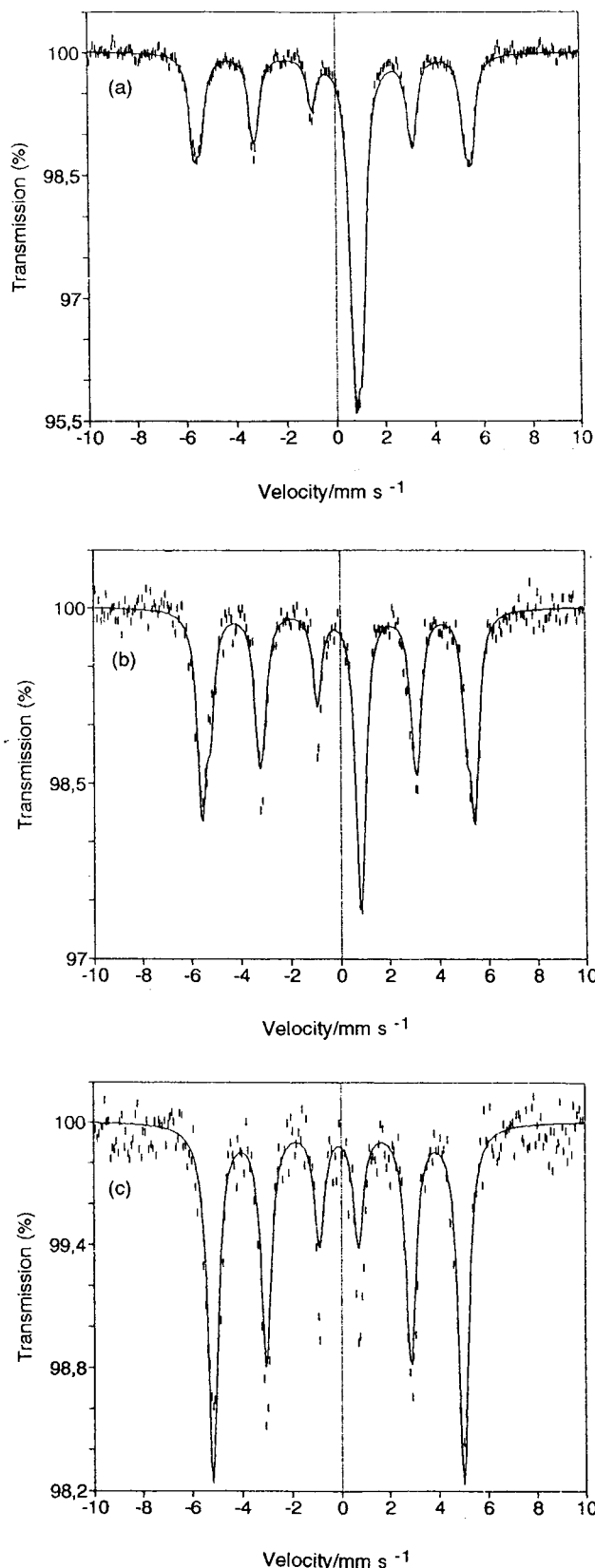
Fig. 7 RT ^{57}Fe Mössbauer spectra of the Fe/Co/Ni–MgO nano-composite powders prepared by reduction at 1100 (a), 1200 (b) or 1300 °C (c); the CS value of natural Fe is equal to -0.15 mm s^{-1}.

Table 1 RT ^{57}Fe Mössbauer parameters of the different iron species present in the Fe/Co/Ni–MgO nanocomposite powders prepared by reduction at 1100, 1200 or 1300 °C; H = hyperfine field/kG; CS = centre shift/mm s^{-1}; Δ_{EQ} = quadrupole splitting/mm s^{-1}; Γ = half width at half height/mm s^{-1}; P = proportion (%); ferro = ferromagnetic

Nanocomposite	Iron species	Mössbauer parameters				
		H	CS	Δ_{EQ}	Γ	P
R1100	Fe^{2+}	—	1.05	0.33	0.22	44
	ferro Fe/Co/Ni	362	0.04	—	0.19	25
	alloy(s)	344	0.04	—	0.24	31
R1200	Fe^{2+}	—	0.99	0.19	0.21	18
	ferro Fe/Co/Ni	352	0.04	—	0.22	57
	alloy(s)	329	0.06	—	0.20	25
R1300	ferro Fe/Co/Ni alloy(s)	326	0.03	—	0.25	100

the hyperfine field distribution which is known to exist in γ-Fe/Ni alloys.[16,25–29] However, the present values are signifi-cantly higher the peaks reported for γ-Fe/Ni-MgAl$_2$O$_4$ nanocomposites (300 and 240 kG),[16] which could reflect that the alloy particles also contain some cobalt. Indeed, a RT hyperfine field equal to 365 kG has been measured for Fe$_{0.65}$Co$_{0.35}$–MgAl$_2$O$_4$ nanocomposite powders[16] and Johnson et al.[30] have reported a nearly constant value (365 kG) in the Fe$_{0.80}$Co$_{0.20}$–Fe$_{0.65}$Co$_{0.35}$ composition range. It is also note-worthy that a singlet corresponding to a paramagnetic γ-Fe/Ni phase is not detected, in contrast to previous results on Fe$_{0.65}$Ni$_{0.35}$-MgO[14] and Fe$_{0.65}$Ni$_{0.35}$-MgAl$_2$O$_4$ nanocomposite powders.[16] This could also point to the presence of cobalt in the alloy particles.

TEM observations. TEM observations of the nanocomposite powders have revealed that the size of the MgO matrix grains is of the order of a few hundreds of nanometers. The metallic particles dispersed in the MgO matrix have a bimodal size distribution (Fig. 8). The size of the metal particles in the two populations (noted P_1 and P_2) are presented in Table 2. As
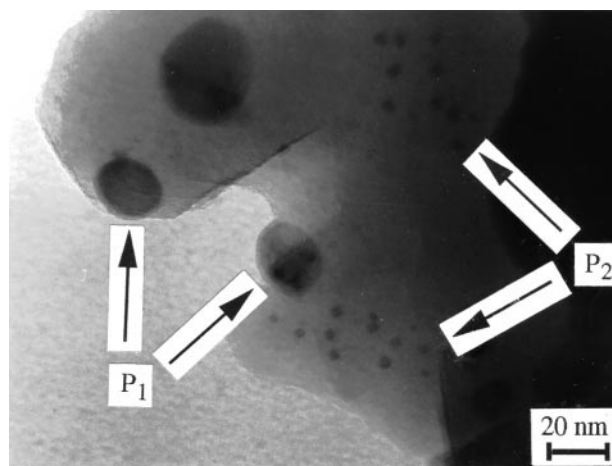

Fig. 8 TEM image of the Fe/Co/Ni–MgO nanocomposite powder prepared by reduction at 1100 °C. P_1 = Population of large metal particles; P_2 = population of small metal particles.

Table 2 Size ($d \pm 10\%$/nm) of the metal alloy particles present in the two populations (P_1, P_2) observed in the Fe/Co/Ni–MgO nanocom-posite powders prepared by reduction at 1100, 1200 or 1300 °C; $<d>$ denotes the average size

Nanocomposite	P_1	P_2
R1100	$20 < d < 95$, $<d> = 40$	$d \leqslant 12$
R1200	$35 < d < 280$, $<d> = 110$	$d \leqslant 15$
R1300	$90 < d < 380$, $<d> = 180$	$d \leqslant 20$

4.7% of the total iron content). Regarding the metallic phase(s), two sextets have been used to fit the spectra of R1100 and R1200. The hyperfine fields are equal to 362 and 344 kG in R1100 and 352 and 329 kG in R1200. In both cases, these particular values could reflect the most intense peaks in

the reduction temperature is increased from 1100 to 1300 °C the proportion of the large P_1 particles increases to the detriment of the small P_2 particles. The large metal particles (P_1) are approximately spherical and are located at the surface of the MgO grains (Fig. 8). The size distribution and the average size of the metal particles were derived from the measurement of the size of about 90 particles pictured on the original TEM negatives. The increase of the average size of the P_1 particles from 40 to 180 nm with the reduction temperature is attributed to an increased proportion of metallic phase on the one hand and to the coalescence of the metal particles on the other hand. Indeed, increasing the reduction temperature (notably from 1100 to 1200 °C) provokes a widening of the size distribution and the formation of much larger particles, several hundreds of nanometers in size. Compared to previous studies,[13,14] it appears that the evolution of the present materials is more similar to that observed for Fe–MgO than for $Fe_{0.65}Ni_{0.35}$–MgO. Indeed, in the latter specimen, the major size and size distribution increases occur between 1200 and 1300 °C. In line with the Mössbauer spectroscopy results, this could indicate that the presence of cobalt offsets the hampering effect of nickel on the reduction of the iron species and thus favours the formation of Fe/Co/Ni alloy particles and their growth at lower temperatures than in the case of Fe/Ni alloys.

The P_2 metal particles are much smaller ($\leqslant 20$ nm) and are either spherical, cubic or parallelepipedic in shape. The electron diffraction pattern [Fig. 9(a)] recorded on an area containing

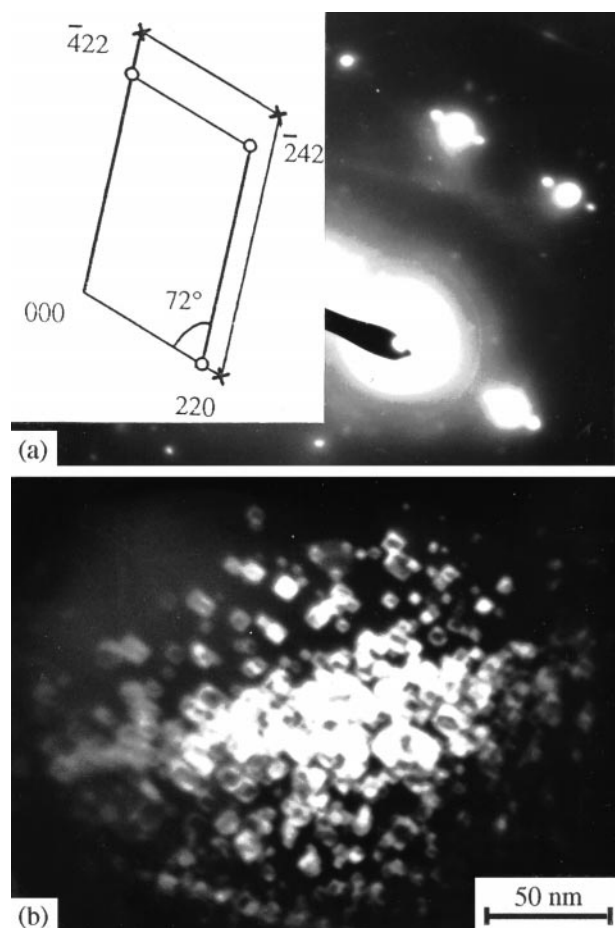both MgO and these metal nanoparticles reveals an alignment according to several directions of the diffraction spots corresponding to (hkl) MgO and ($h'k'l'$) γ-alloy planes. The corresponding dark field image [Fig. 9(b)] using a (220) γ-alloy spot as operative reflection reveals that all the nanoparticles are in contrast. The relationships of common orientation between MgO and the metal particles observed on the electron diffraction pattern for the different powders are reported in Table 3. These results show that there is a perfect cube/cube orientation relationship between MgO and the metal particles in the present R1100, R1200 and R1300 powders. The cube/cube orientation has been observed in $Fe_{0.65}Ni_{0.35}$–MgO nanocomposite powders.[14] The present results as well as a comparison with earlier studies on Fe–Al_2O_3 nanocomposite powders[12,31] could indicate that the P_2 nanoparticles grow epitaxially inside the grains of the MgO matrix. This could account for the moderate growth observed upon the increase in reduction temperature.

TEM EDX microanalyses. TEM EDX microanalyses performed on metal particles larger than 20 nm in size and located on the edges of the MgO grains (P_1 particles) have revealed the presence of Fe/Co/Ni alloy particles with different compositions (Table 4). Three populations of metal particles (denoted A, B and C hereafter) have been observed in the R1100 specimen. Particles in population A, which account for *ca.* 70% of the investigated particles, have an iron content in the 57–63 at.% range, a cobalt content slightly lower than the target one (*ca.* 31 at.%) and a nickel content markedly lower than the desired one (*ca.* 22 at.%). Comparing population B, which represents a smaller proportion of particles, to A shows that the iron content is slightly lower (50–54 at.%) whereas those of Co and Ni are higher B. The same evolutions are observed from populations B to C, which represent a still smaller proportion of particles. Thus, C particles have a composition close to the desired one ($Fe_{0.47}Co_{0.31}Ni_{0.22}$). It is noteworthy that only one population of metal particles (D) is observed in the R1200 powder. The contents of Fe, Co and Ni are in the 53–56, 30–32 and 13–16 at.% ranges, respectively, which fall in between those measured for populations A and B. The cobalt content is the desired one, but those of Fe and Ni are too high and too low, respectively. In contrast, powder R1300 presents a large proportion (*ca.* 65%) of alloy particles with a composition (E) very close to the desired one. However, two more populations (F and G) are observed in small

Fig. 9 (a) Electron diffraction pattern recorded on an area containing both MgO and the small metal particles (P_2 population) in the powder prepared by reduction at 1100 °C. The inset shows diffraction spots corresponding to (hkl) MgO [○] and ($h'k'l'$) γ-alloys [×] planes (the other spots are attributed to double diffraction, zone axis [1$\bar{1}$3]). (b) The corresponding TEM image (in the dark-field mode with 220 alloy spot as operative reflection) of the γ alloy (Fe/Ni and/or Fe/Co/Ni) particles dispersed inside the MgO matrix.

Table 3 Cube/cube epitaxial relations between the alloy nanoparticles (γ-Fe/Ni and/or γ-Fe/Co/Ni) and the MgO matrix present in the Fe/Co/Ni–MgO nanocomposite powders prepared by reduction at 1100, 1200 or 1300 °C; γ stands for γ alloy

Nanocomposite	Relations of epitaxy		
R1100	(220)γ//(220)MgO	($\bar{2}$42)γ//($\bar{2}$42)MgO	[1$\bar{1}$3]γ//[1$\bar{1}$3]MgO
R1200	(200)γ//(200)MgO	(131)γ//(131)MgO	[0$\bar{1}$3]γ//[0$\bar{1}$3]MgO
R1300	(200)γ//(200)MgO	(220)γ//(220)MgO	[001]γ//[001]MgO

Table 4 Composition of the different population of Fe/Co/Ni alloy particles present in the Fe/Co/Ni–MgO nanocomposite powders prepared by reduction at 1100, 1200 or 1300 °C

Nanocomposite	Code, proportion	Metal content (±5 at.%)		
		Fe	Co	Ni
R1100	A, great	57–63	25–29	8–15
	B, small	50–54	27–35	15–19
	C, very small	43	33	24
R1200	D	53–56	30–32	13–16
R1300	E, great	44–48	31–33	21–24
	F, very small	43.5	27	29.5
	G, small	31–37	25–33	36–38

proportions and present an iron content lower and a nickel content higher than in the target composition. Although no correlation could be made between the composition and the size of a particle, it is probable that the formation of populations different in size and composition are related. In addition, spot analyses were performed for R1300 on areas of the matrix appearing devoid of metal particles. Very small contents of residual iron (*ca.* 4.7), cobalt (*ca.* 1) and nickel (*ca.* 4%) ions have been detected. The present results, in line with those obtained for Fe/Ni–MgO powders,[14] seem to indicate that the P_1 alloy particles become enriched in nickel upon increasing reduction temperature. In contrast, the $Fe_{0.65}Ni_{0.35}$ particles dispersed in $MgAl_2O_4$ became enriched in iron upon increasing reduction temperature up to 1000 °C, which was adequate for the obtention of alloy particles with the desired composition and a very narrow composition distribution.[16] An explanation for this discrepancy could be that the smaller P_2 particles, that were not analysed in the present work, are sufficiently rich in nickel that one obtains a result similar to that of $Fe_{0.65}Ni_{0.35}$–$MgAl_2O_4$ when taking into account all the $P_1 + P_2$ particles. However, this seems unlikely since no corresponding peak is detected on the X-ray pattern of specimen R1100. Another explanation could be that the Fe^{2+} ions are more easily reduced than the Ni^{2+} ions in the MgO matrix, contrary to what is observed in a $MgAl_2O_4$ matrix, because of the clustering of iron ions and vacancies that occurs in the MgO-based solid solution. Cobalt has been shown to be reduced to the metallic state at a temperature about 100 °C lower than iron and nickel in a $MgAl_2O_4$ matrix and has been found to promote the reduction of the Fe^{2+} ions.[16] It is proposed that cobalt has the same role in MgO, but its influence on the reduction of the Ni^{2+} ions is unknown.

Conclusion

A mixed oxalate β-$Mg_{0.896}Fe_{0.047}Co_{0.034}Ni_{0.023}C_2O_4 \cdot 2H_2O$ of well controlled size (*ca.* 1 μm) and morphology was obtained by coprecipitation. Thermal decomposition at 500 °C in the appropriate $H_2/H_2O/N_2$ atmosphere allowed us to prepare the corresponding quaternary solid solution between MgO, FeO, CoO and NiO. Further calcination at 800 °C decreases the specific surface area but does not provoke any phase partitioning. A study of the selective reduction of this solid solution in a H_2 atmosphere has brought to light the very high stability of the Fe^{2+}, Co^{2+} and notably Ni^{2+} when substituted for Mg^{2+} in the MgO rocksalt lattice. Indeed, it is necessary to perform the reduction at 1300 °C fully to reduce the transition metal ions. The alloy particles are either distributed as relatively large particles (tens to hundreds of nanometers) at the surface of the MgO grains or as much smaller particles (≤20 nm) probably located inside the matrix grains and epitaxied with it. Analysis of the large surface particles indicates that the composition distribution is fairly broad in the powders prepared by reduction at 1100 and 1300 °C. In the former specimen the metal particles are too rich in Fe compared to the target composition ($Fe_{0.47}Co_{0.31}Ni_{0.22}$). In the latter more than half the studied particles have the desired composition, but the other particles are too rich in Ni. In contrast, the composition distribution is much narrower in the powder prepared by reduction at 1200 °C, although the particles are still too poor in Ni. It is proposed that properly adjusting the transition metal contents in the oxide powder and the reduction temperature could allow one to prepare alloy particles with both the desired composition and a narrow composition distribution. The microstructure of the present Fe/Co/Ni–MgO composite powders is fairly complex, but it is anticipated that dense materials prepared from these powders could present interesting physical and mechanical properties.

References

1 D. Chakravorty, *Bull. Mater. Sci.*, 1992, **15**, 411.
2 S. Komarneni, *J. Mater. Chem.*, 1992, **2**, 1219.
3 R. Roy, *Mater. Res. Soc. Symp. Proc.*, 1993, **286**, 241.
4 Ch. Laurent and A. Rousset, *Key. Eng. Mater.*, 1995, **108–110**, 405.
5 D. Chakravorty, *Sadhana*, 1988, **13**, 13.
6 P. Matteazzi and G. Le Caër, *J. Am. Ceram. Soc.*, 1992, **75**, 2749.
7 L. A. Chick, G. D. Maupin and L. R. Pederson, *NanoStruct. Mater.*, 1994, **4**, 603.
8 X. Devaux, Ch. Laurent and A. Rousset, *NanoStruct. Mater.*, 1993, **2**, 339.
9 Ch. Laurent, A. Rousset, M. Verelst, K. R. Kannan, A. R. Raju and C. N. R. Rao, *J. Mater. Chem.*, 1993, **3**, 513.
10 M. Verelst, K. R. Kannan, G. N. Subbanna, C. N. R. Rao, M. Brieu and A. Rousset, *Mater. Res. Bull.*, 1993, **28**, 293.
11 Ch. Laurent, J. J. Demai, A. Rousset, K. R. Kannan and C. N. R. Rao, *J. Mater. Res.*, 1994, **9**, 229.
12 Ch. Laurent, Ch. Blaszczyk, M. Brieu and A. Rousset, *NanoStruct. Mater.*, 1995, **6**, 317.
13 V. Carles, M. Brieu, J. J. Demai and A. Rousset, in *Fourth Euro-Ceramics Vol. 1*, ed. C. Galassi, Gruppo Editoriale Faenza Editrice S. p. A., Faenza, Italy, 1995, p. 323.
14 V. Carles, M. Brieu and A. Rousset, *NanoStruct. Mater.*, 1997, **8**, 529.
15 O. Quénard, Ch. Laurent, M. Brieu and A. Rousset, *NanoStruct. Mater.*, 1996, **7**, 497.
16 O. Quénard, E. De Grave, Ch. Laurent and A. Rousset, *J. Mater. Chem.*, 1997, **7**, 2457.
17 A. Chatterjee, D. Das, D. Chakravorty and K. Choudhury, *Appl. Phys. Lett.*, 1990, **57**, 1360.
18 K. Kusaka, N. Wada and A. Tasaki, *Jpn. J. Appl. Phys.*, 1969, **8**, 599.
19 V. Carles and A. Rousset, *Solid State Ionics*, 1996, **83**, 309.
20 V. Carles, Doctoral Thesis, Toulouse, 1995, 248pp.
21 H. Pezerat, J. Dubernat and J. P. Lagier, *C. R. Hebd. Seances Acad. Sci. Sér. C*, 1968, **266**, 1357.
22 R. Deyrieux and A. Peneloux, *Bull. Soc. Chim. Fr.*, 1969, **8**, 2675.
23 G. A. Waychunas, *J. Mater. Sci.*, 1983, **18**, 195.
24 P. Tailhades, Doctoral Thesis, Toulouse, 1988, 174pp.
25 U. Gonser, S. Nasu and W. Kappes, *J. Magn. Magn. Mater.*, 1979, **10**, 244.
26 S. Tomiyoshi, H. Yamamoto and H. Watanabe, *J. Phys. Soc. Jpn.*, 1971, **30**, 1605.
27 H. Rechenberg, L. Billard, A. Chamberod and M. Natta, *Phys. Chem. Solids*, 1973, **34**, 1251.
28 H. Ullrich and J. Hesse, *J. Magn. Magn. Mater.*, 1984, **45**, 315.
29 I. Ortalli, A. Vera, G. Fratucello and F. Ronconi, *Hyperfine Interact.*, 1986, **28**, 1025.
30 C. E. Johnson, M. S. Ridout and T. E. Cranshaw, *Proc. Phys. Soc.*, 1963, **81**, 1079.
31 X. Devaux, Ch. Laurent, M. Brieu and A. Rousset, *J. All. Compd.*, 1992, **188**, 179.

Paper 8/09642B